Active Junction Temperature Control of IGBT Based on Adjusting the Turn-off Trajectory

Bo Wang, Luowei Zhou, *Senior Member, IEEE*, Yi Zhang, Kaihong Wang, Xiong Du, *Member, IEEE*, and Pengju Sun, *Member, IEEE*

***Abstract*—The junction temperature fluctuation of an insulated-gate bipolar transistor (IGBT) is the most important factor of its aging failure, and smoothing the fluctuation is an effective way to improve the life of an IGBT. The existing methods for smoothing the fluctuation by active junction temperature control are not yet ready wide application, and exploring the different approaches to active junction temperature control is a hot topic. This paper presents a method of active junction temperature control that shifts the turn-off trajectory of an IGBT to adjust the IGBT turn-off loss for smoothing the junction temperature. The relationship between parameters of the adjusting circuit and turn-off loss is analyzed. On the basis of this analysis, a method of estimating the smoothing ability for the proposed active junction temperature control is deduced. Using an IGBT installed in a 1.2-MW direct-drive wind power converter as an example, the evaluation result shows that the proposed method can completely smooth the junction temperature fluctuation caused by a 40% rated load fluctuation. Finally, a low-power experiment is carried out.**

***Index Terms*—Insulated-gate bipolar transistor (IGBT), smoothing ability, smoothing junction temperature, turn-off trajectory.**

I. Introduction

IN RECENT years, with the large number of power electronic devices placed into service in new energy power generation, electric vehicles, and other nonstationary operating conditions, the reliability of power electronic devices has become increasingly prominent [1]–[3]. The insulated-gate bipolar transistor (IGBT) is the core component of converters, and it plays a decisive role for the safety and reliability. The Coffin–Manson and Bayerer IGBT life model shows that the main reason for IGBT aging failure is the thermal stress caused by the junction temperature fluctuation. Due to different thermal expansion coefficients of different layers between the chip and the baseplate in the IGBT module, the junction temperature fluctuation can cause different levels of expansion in different layers so that the thermal stress shock is generated, which will lead to IGBT fatigue aging [4]–[6].

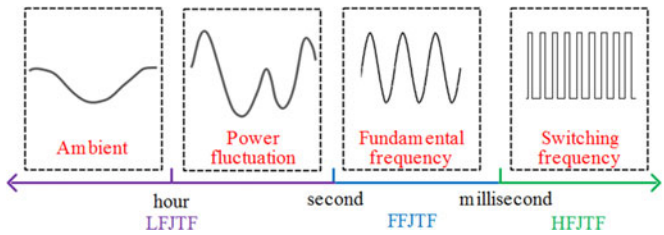

Fig. 1. Classification of junction temperature fluctuations.

The main junction temperature fluctuation of an IGBT can be generally classified into three categories according to the frequency: high-frequency junction temperature fluctuation (HFJTF), fundamental-frequency junction temperature fluctuation (FFJTF), and low-frequency junction temperature fluctuation (LFJTF), as shown is Fig. 1. HFJTF is caused by closing and opening of the IGBT in a switching period, its frequency coincides with the switching frequency; FFJTF exists in the sinusoidal converter, since the current flows through the IGBT only in half fundamental period, and its frequency coincides with the fundamental frequency of the sinusoidal converter; LFJTF is mainly caused by the loading profile whose frequency is lower than the fundamental frequency, such as random changes in the wind speeds in a wind power converter, and the ambient temperature fluctuations may lead to junction temperature fluctuations with the much lower frequency. The range of HFJTF is very small due to the frequency of HFJTF is usually over kilohertz so that it has a little influence on the lifetime of an IGBT [7]. The influence of FFJTF on IGBT lifetime is mainly related to its frequency. The IGBTs' life consumption caused by LFJTF and FFJTF is on the same level if the frequency of FFJTF is low, such as the generator-side converter of wind power (the base frequency is 16 Hz). The FFJTF has a little effect on IGBT lifetime when the frequency of BFJTF is high, such as the grid-side converter of wind power (the base frequency is 50 Hz), then the LFJTF is the most important factor for consuming the IGBT lifetime [6], [8]. Therefore, smoothing LFJTF plays a significant role in reducing the life consumption of an IGBT.

At present, a lot of active junction temperature control methods have been proposed to reduce LFJTF. The basic idea of existing active junction temperature control methods is to

Manuscript received June 6, 2017; revised August 4, 2017; accepted August 26, 2017. Date of publication September 4, 2017; date of current version March 5, 2018. This work was supported in part by the National Nature Science Foundation of China under Grant 51137006, in part by the National Nature Science Foundation of China under Grant 51577020, and in part by the Chongqing University Postgraduate's Innovation Project (CYB15034). Recommended for publication by Associate Editor A. Lindemann. *(Corresponding author: Luowei Zhou.)*

The authors are with the State Key Laboratory of Power Transmission Equipment and System Security and New Technology, School of Electrical Engineering, Chongqing University, Chongqing 400044, China (e-mail: wbo@cqu.edu.cn; zluowei@cqu.edu.cn; 393651679@qq.com; 1205546969@qq.com; duxiong@cqu.edu.cn; spengju@163.com).

Color versions of one or more of the figures in this paper are available online at http://ieeexplore.ieee.org.

Digital Object Identifier 10.1109/TPEL.2017.2749383

compensate the loss of the IGBT when the power of the converter is reduced and it can be implemented in several major ways. A junction temperature smoothing method based on the switching frequency has been proposed [9], [10], and this method does not need additional hardware. However, it cannot individually adjust the loss of each IGBT in the bridge topology. In [11], a junction temperature smoothing method based on the gate driving voltage has been proposed, and this method can individually adjust the loss of each power device. However, there are the very high demands of dynamic response and control accuracy in the control circuit so that the drive control method needs to consider implementing the cost problem. On the other hand, some literature papers have proposed junction temperature smoothing methods for a parallel converter system. In [12], a junction temperature smoothing method based on a reactive current cycling is proposed, which utilizes the reactive power delivered in the parallel converter to compensate the loss. However, it can only be applied to a parallel converter system and it increases the thermal load of the diode. What's more, there are some other methods for a specific application, and played a better effect. For example, Ma and Blaabjerg [13] increased the lifetime of the three level neutral-point-clamped wind power inverter under low-voltage crossing, which adjusted the current path by the redundant short vectors at the inner hex of the space vector diagram to reduce the thermal stress of the neutral-point-clamped diode. In fast-varying irradiance environments, a method is presented to reduce the maximum temperature derivative, which at the same time reduces the thermal cycle. This concept was explored in [14], where the duty cycle of a dc/dc converter for photovoltaic system was actively modified in order to limit the maximum junction temperature derivative in the presence of irradiation changes. In order to reduce the impact of ambient temperature fluctuations, speed of the cooling fan is controlled [15]. In a word, those methods for specific applications can effectively reducing the thermal load of the IGBT, but they are not suitable to other conditions.

In summary, smoothing the LFJTF can significantly improve the life expectancy of an IGBT. However, there are many problems in the existing methods for real application. Hence, more feasible methods of active junction temperature control need to be explored. In this paper, an active junction temperature control method is proposed which compensates the internal loss of an IGBT by the turn-off loss. The turn-off loss is adjusted by shifting the IGBT turn-off trajectory and the turn-off trajectory is shifted by the turn-off trajectory adjustment circuit (TTAC) as detailed in this paper. It has the characteristics of individually control the junction temperature of each IGBT, providing simple control and having a little effect on the dead time between the upper and lower switches.

II. Smoothing the Junction Temperature by Turn-off Loss

The power loss of an IGBT is mainly composed of the conduction power loss $P_{\rm con}$, the turn-on power loss $P_{\rm swon}$, and the turn-off power loss $P_{\rm swoff}$ [16]. Here, $P_{\rm con}$ is related to the load current $I_{\rm load}$ and the junction temperature T_j; $P_{\rm swon}$ and $P_{\rm swoff}$ are related to the dc-bus voltage $V_{\rm dc}$ and the switching frequencies f_s, $I_{\rm load}$, and T_j. Therefore, the IGBT power loss $P_{\rm loss}$ can be expressed as follows:

$$P_{\rm loss}(V_{\rm dc}, I_{\rm load}, T_j, f_s) = P_{\rm con}(I_{\rm load}, T_j) + P_{\rm swon}(V_{\rm dc}, I_{\rm load}, T_j, f_s) + P_{\rm swoff}(V_{\rm dc}, I_{\rm load}, T_j, f_s). \quad (1)$$

Generally, the switching loss accounts for a large proportion of the total loss of a high-power IGBT module, e.g., the IGBT module 2MBI1000VXB-170EA-50 ($V_{\rm ce} = 170$ V, $I_{\rm ce} = 1000$ A) of Fuji Electric. The proportion of each loss can be acquired by the loss simulation software of Fuji Electric [17]. Under the rated operating condition, $P_{\rm con}$ accounts for 24.8%, $P_{\rm swon}$ accounts for 30.4%, and $P_{\rm swoff}$ accounts for 44.8% of the total loss according to the simulation results. Moreover, $P_{\rm con}$ is only determined by $I_{\rm load}$, which is not easy to adjust; the actual $P_{\rm swon}$ is less than the calculated value due to the influence of parasitic inductance; and $P_{\rm swoff}$ accounts for a large proportion of the total loss so that it is suitable for smoothing the LFJTF of an IGBT.

An example to illustrate active junction temperature control by the turn-off loss is given as follows. The conduction loss is exactly the same in Fig. 2(a) and (b), respectively, which means that the load fluctuation is the same. In Fig. 2(a), the loss of the IGBT is not adjusted so that the junction temperatures fluctuate with the load fluctuations. In Fig. 2(b), the turn-off loss has been online adjusted in real time when the power of the converter is reduced, fluctuations of the IGBT internal losses are compensated so that the junction temperature fluctuations are smoothed by adjusting the turn-off loss.

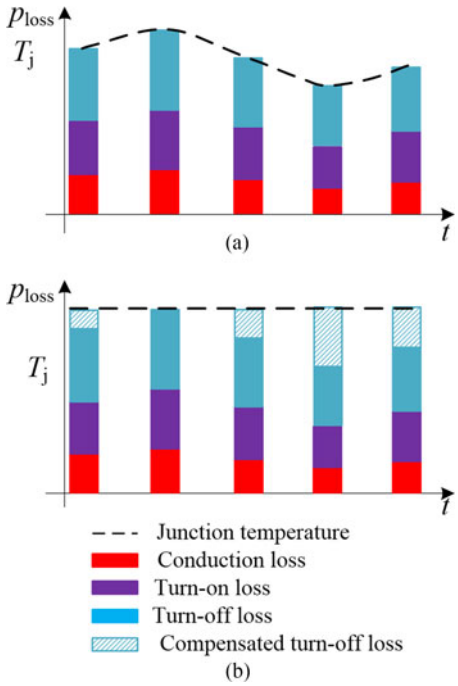

Fig. 2. Smoothing junction temperature fluctuation of IGBT by turn-off loss. (a) Without adjusting the turn-off loss. (b) With adjusting the turn-off loss.

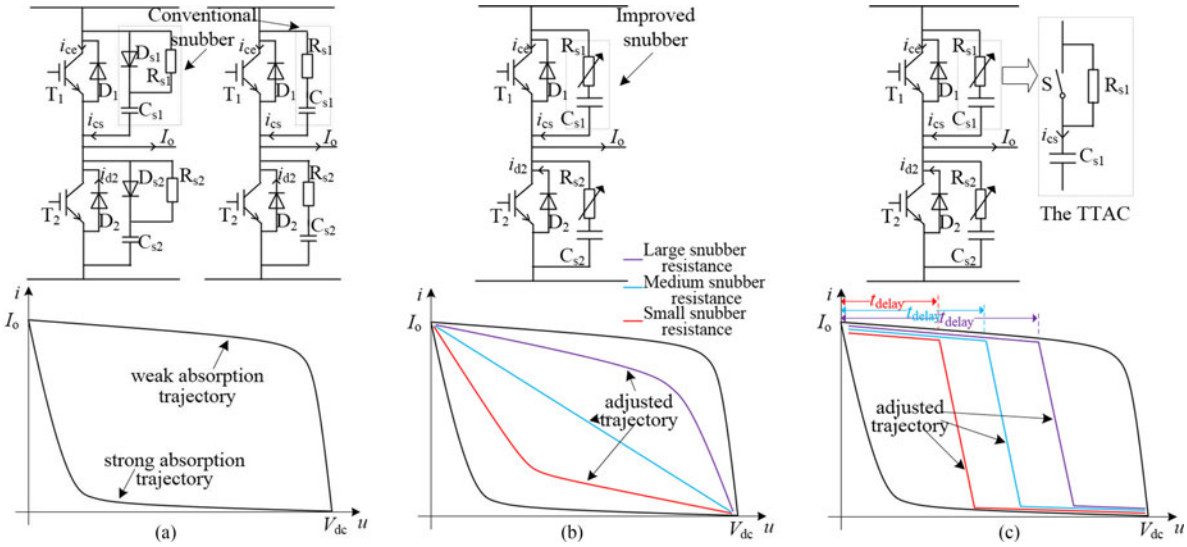

Fig. 3. Snubber and the turn-off trajectory. (a) Conventional snubber. (b) Improved snubber. (c) TTAC.

As is known, if an IGBT turns off with a conventional *RCD* snubber of a suitable capacitor, the IGBT will work on the strong absorption trajectory with a small turn-off loss; if an IGBT turns off with a conventional *RC* snubber of a large enough resistor, the IGBT will work on the weak absorption trajectory with a large turn-off loss, as shown in Fig. 3(a). The parameters of the conventional snubber are fixed, so the turn-off loss of the IGBT is also fixed. During the operation of the converter, if the snubber parameters can be online adjusted in real time as the power of the converter reduces, the reduction loss of the IGBT will be compensated, then the junction temperature can maintain stable. In this paper, an improved snubber is presented, the diode and resistor in the conventional *RCD* snubber is replaced by the adjustable resistance. With the change of the resistance value, the turn-off trajectory of the IGBT is changed between the weak absorption trajectory and the strong absorption trajectory, as shown in Fig. 3(b) so that the turn-off loss of the IGBT can be adjusted.

However, generally the power of digital adjustable resistance is very small, and it cannot be used for a snubber, such as a digital potentiometer. In this paper, an equivalent adjustable resistor is proposed as shown in the dashed box of Fig. 3(c), it is the TTAC. An auxiliary switch S is connected in parallel to the snubber resistor $R_{\rm s1}$. The TTAC shifts the IGBT turn-off trajectory by controlling delay closed time of S $t_{\rm delay}$ during the turn-off process of the IGBT, as shown in Fig. 3(c). It is not difficult to understand, the influence of the turn-off trajectory, as show in Fig. 3(b) and (c), on the turn-off loss is equivalent. The principle of the TTAC and the quantitative relation between $t_{\rm delay}$ and the turn-off loss will have a detailed explanation in the follow sections.

III. Working Principle of the TTAC

In order to illustrate the working principle of the TTAC, we assume that an IGBT works with the TTAC as show in Fig. 3(c). When the IGBT turns off, the charging current $i_{\rm cs}$ of snubber capacitor C_{s1} has two paths, i.e., through S or R_{s1}, as shown in Fig. 4(a) and (b); when the IGBT turns on, C_{s1} is discharged through R_{s1} by opening S in order to limit the discharge current peak, as shown in Fig. 4(c).

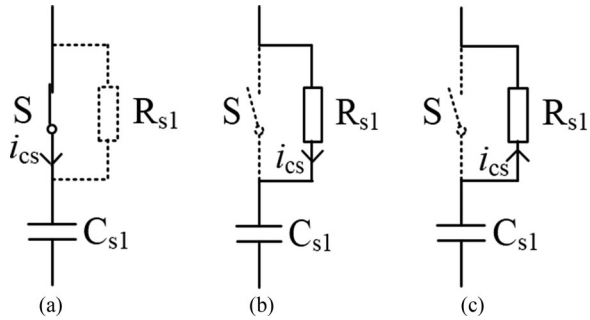

Fig. 4. Charge and discharge path of the capacitor. (a) Charging path through S. (b) Charging path through $R_{\rm s1}$. (c) Discharging path through $R_{\rm s1}$.

In Fig. 3(c), if S is kept closing during the T_1 turn-off period, the TTAC will be equivalent to the conventional *RCD* snubber. Its turn-off waveform is shown by the dotted line in Fig. 5(a). The turn-off process of the IGBT is explained as follows. T_1 begins to turn off at the t_0 moment. Its collector current $i_{\rm ce}$ falls rapidly from the load current $I_{\rm o}$, and its collector–emitter voltage $v_{\rm ce}$ slowly rises from $v_{\rm cesat}$ to the dc-bus voltage $V_{\rm dc}$. In this state, the IGBT works on the strong absorption trajectory, as shown in Fig. 3(a), and the turn-off loss of IGBT is small.

If S is kept opening during the T_1 turn-off period, the TTAC will be equivalent to a *RC* snubber. If the snubber resister is large enough, IGBT will turn off with the hard switching, its turn-off waveform is shown by the solid line in Fig. 5(a). The turn-off process of the IGBT is explained as follows. T_1 begins to turn off at the t_0 moment. The load current $I_{\rm o}$ shunts to the snubber capacitor through the snubber resistor so that $i_{\rm ce}$ declines very slowly, and the $v_{\rm ce}$ begins to rise at the same time. At the t_1 moment, $v_{\rm ce}$ rises to $V_{\rm dc}$, and $i_{\rm ce}$ can rapidly decline. In this state, the IGBT works on a weak absorption trajectory, as shown in Fig. 3(a), and the turn-off loss of the IGBT is large.

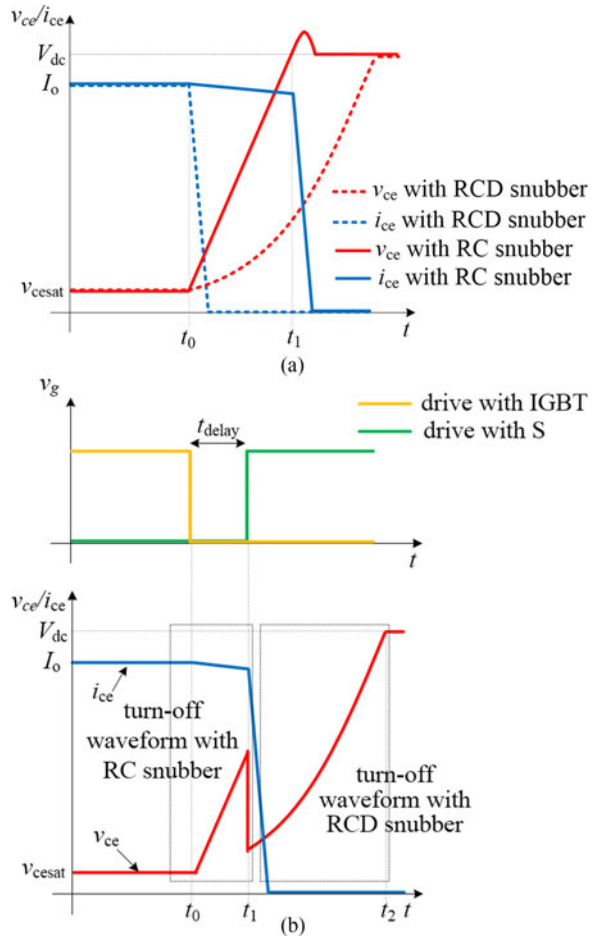

Fig. 5. Turn-off waveform of IGBT. (a) Turn-off waveform with *RCD* snubber and *RC* snubber. (b) Turn-off waveform with the TTAC.

The turn-on signal of S delays the turn-off signal of the main switch T_1 for $t_{\rm delay}$. The waveform of T_1 is shown in Fig. 5(b), and the detail of the waveform is explained as follows. S is kept opening at the t_0 moment. The turn-off waveform of the IGBT is the same as when the IGBT turns off on the weak absorption trajectory. S is closed after $t_{\rm delay}$, $R_{\rm s1}$ is shorted, and the turn-off waveform of the IGBT is the same as when the IGBT turns off on the strong absorption trajectory. This means the IGBT turn-off trajectory can be shifted by controlling the delay closed time $t_{\rm delay}$ of S, as shown in Fig. 3(c). With the different $t_{\rm delay}$, the turn-off trajectory is also different, the longer the $t_{\rm delay}$, the longer the IGBT turns off on the weak absorption trajectory, and the larger the turn-off loss as well.

What's more, if the auxiliary switch is short, then the TTAC is a *RCD* snubber; if the auxiliary switch is broken, then the TTAC is a *RC* snubber, as shown in Fig. 6, neither of them will affect the normal operation of the main circuit. So it does not introduce a new security risk.

IV. Relationship Between Parameters of the TTAC and Turn-off Loss

In the TTAC, the resistor and capacitor will affect the maximum and minimum turn-off losses of the IGBT, which means

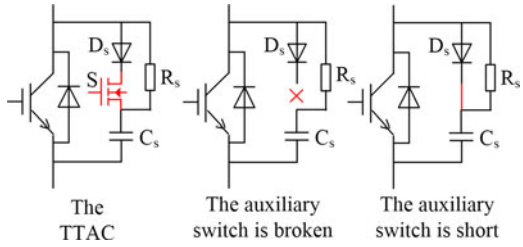

Fig. 6. Possible faults of auxiliary switches.

that the resistor and capacitor will affect the adjustment range of the TTAC. This section will derive the relationship among the resistor, capacitor, and the turn-off loss. The results can be used to determine the resistance and capacitance values of the TTAC and estimate the adjustment range of the TTAC. The relationship between $t_{\rm delay}$ and the turn-off loss will also be deduced in this section.

A. Effect of Resistance on Turn-off Loss

If S is kept opening during the T_1 turn-off period, the TTAC can be equivalent to a RC snubber, and $i_{\rm ce}$ will shunt slightly to the *RC* branch due to the snubber resistor. The parasitic inductor on the *RC* branch is ignored to simplify the analysis. There are four main modes during the turn-off of the IGBT, and the typical waveforms are shown in Fig. 7. The relevant equivalent circuits are shown in Fig. 8.

Mode I [t_0, t_1]: During this time interval, the gate voltage of T_1 $v_{\rm ge}$ starts falling from $V_{\rm ge}$ to the holding voltage $V_{\rm gp}$, T_1 remains on state, the collector–emitter voltage of T_1 $v_{\rm ce}$ is the saturation voltage $V_{\rm cesat}$, and the collector current of T_1 $i_{\rm ce}$ maintains the load current $I_{\rm o}$. At t_1 moment, $v_{\rm ge}$ falls to $V_{\rm gp}$.

Mode II [t_1, t_2]: During this time interval, $i_{\rm ce}$ slowly declines, the sum of $i_{\rm ce}$, $i_{\rm cs}$, and $i_{\rm cs2}$ is $I_{\rm o}$, C_{s1} is charged by $i_{\rm cs}$, and C_{s2} is discharged by $i_{\rm cs2}$. Due to the process of C_{s1} charging and C_{s2} discharging being completely symmetrical, $i_{\rm cs}$ is equal to $i_{\rm cs2}$. The relationship between $i_{\rm ce}$ and $i_{\rm cs}$ is as follows:

$$i_{\rm ce} = I_o - 2i_{\rm cs}. \tag{2}$$

$v_{\rm ce}$ rises from $V_{\rm cesat}$ to $V_{\rm dc}$, and the sum of $v_{\rm ce}$ and the collector–emitter voltages of T_2 $v_{\rm ce2}$ is the dc-bus voltage $V_{\rm dc}$. Assuming R_{s1} and C_{s1} are large enough, the voltage on the snubber capacitor can be ignored. Then, $v_{\rm ce}$ is given by

$$v_{\rm ce} = R_{s1}i_{\rm cs} + \frac{1}{C_{\rm cs1}}\int_0^t i_{\rm cs}dt \approx R_{s1}i_{\rm cs}. \tag{3}$$

In this mode, the gate current i_g is mainly for $C_{\rm cg}$ charging. Then, $i_{\rm cg}$, $v_{\rm cg}$ are given by

$$i_{\rm cg} = \frac{v_{\rm ge}}{R_g} \tag{4}$$

$$v_{\rm cg} = \frac{1}{C_{\rm cg}}\int_{t_1}^{t_2} i_{cg}dt. \tag{5}$$

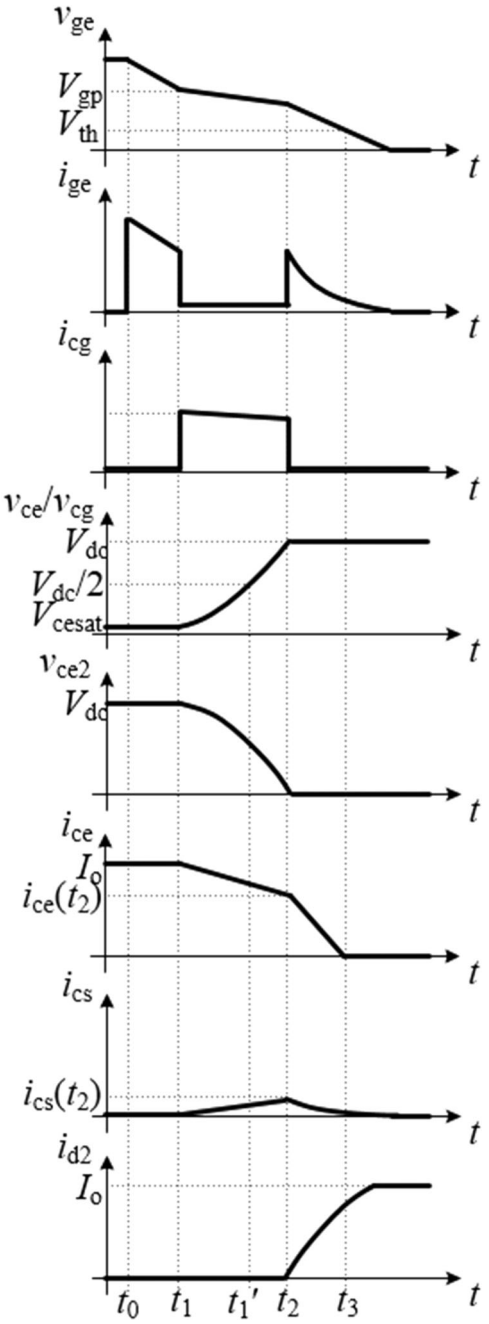

Fig. 7. Typical waveforms of the TTAC.

At t_2 moment, $v_{\rm ce}$ leads to $V_{\rm dc}$ from $V_{\rm cesat}$, and $i_{\rm cs}$ is approximated as a linear change in this mode, which is given by

$$i_{\rm cs}(t) = \frac{i_{\rm cs}(t_2) - i_{\rm cs}(t_1)}{t_2 - t_1} t = \frac{V_{\rm dc} - V_{\rm cesat}}{(t_2 - t_1) R_{s1}} t. \tag{6}$$

According to (2), $i_{\rm ce}$ can be approximated as a linear change as follows:

$$i_{\rm ce}(t) = I_o - 2\frac{V_{\rm dc} - V_{\rm cesat}}{(t_2 - t_1) R_s} t. \tag{7}$$

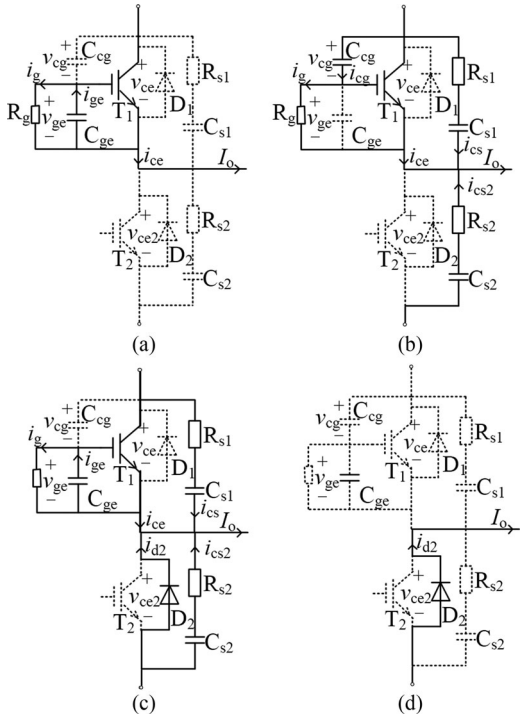

Fig. 8. Operational modes of the TTAC on a leg of bridge topology. (a) Mode I. (b) Mode II. (c) Mode III. (d) Mode IV.

The relationship between $i_{\rm ce}$ and $v_{\rm ge}$ can be acquired through the IGBT datasheet, which can be written as follows:

$$i_{\rm ce} = a v_{\rm ge} + b. \tag{8}$$

Here, a and b are the fitting coefficients.

According to (4), (7), and (8), $i_{\rm cg}$ can be approximated as a linear change as follows:

$$i_{\rm cg} = \frac{I_o - b}{a R_g} - \frac{2V_{\rm dc}}{a R_{s1} R_g (t_2 - t_1)} t. \tag{9}$$

During the process of $v_{\rm ce}$ increasing, $C_{\rm cg}$ will nonlinearly change with the $v_{\rm ce}$. Trivedi and Shenai [18] used the two-points method for determining the value of $C_{\rm cg}$: during $v_{\rm ce}$ from $V_{\rm cesat}$ up to $V_{\rm dc}/2$, the value of $C_{\rm cg}$ is set to $C_{\rm cg}(V_{\rm cesat})$; during $v_{\rm ce}$ from $V_{\rm dc}/2$ up to $V_{\rm dc}$, the value of $C_{\rm cg}$ is set to $C_{\rm cg}\,(V_{\rm dc}/2)$. According to (5), the equations can be written as

$$\begin{cases} \frac{V_{\rm dc}}{2} = \frac{1}{C_{\rm cg(Vcesat)}} \int_{t_1}^{t_1'} i_{\rm cg}\, dt \\ \frac{V_{\rm dc}}{2} = \frac{1}{C_{\rm cg(Vdc/2)}} \int_{t_1'}^{t_2} i_{\rm cg}\, dt. \end{cases} \tag{10}$$

From (9) and (10), the duration of the mode $t_{\rm ur}$ can be acquired as follows:

$$\begin{aligned} t_{\rm ur} &= t_2 - t_1 = (t_1' - t_1) + (t_2 - t_1') \\ &= \frac{a(C_{\rm cg(Vdc/2)} + C_{\rm cg(Vcesat)}) V_{\rm dc} R_g R_{s1}}{2(R_{s1} I_o - R_{s1} b - V_{\rm dc})}. \end{aligned} \tag{11}$$

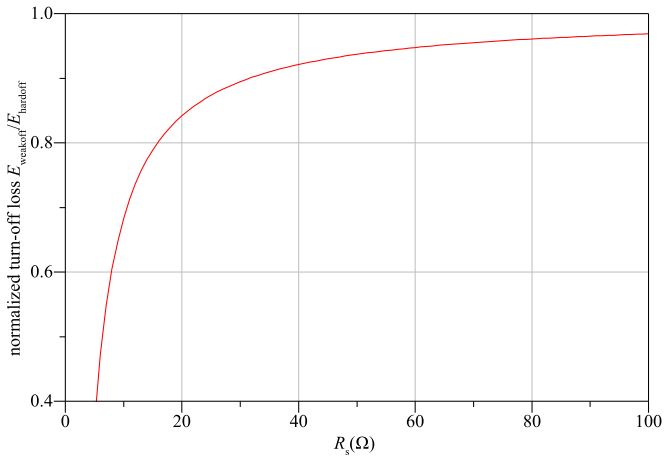

Fig. 9. Relationship between E_{weakoff} and R_s.

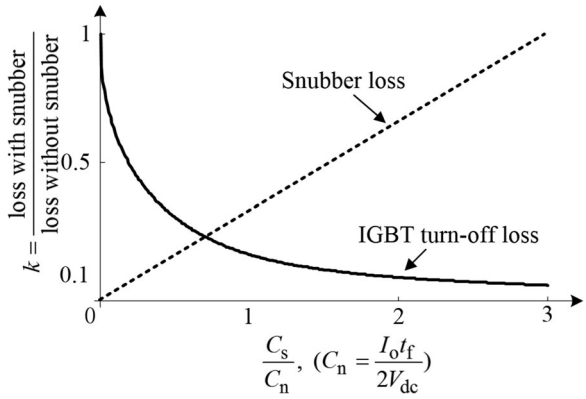

Fig. 10. Relationship between snubber capacitance and the turn-off loss of an IGBT (C_s is the snubber capacitance, I_o is the load current, t_f is the fall time of I_o, and V_{dc} is the dc-bus voltage.)

The power loss during mode II $E_{\mathrm{swoff}(2)}$ can be calculated as follows:

$$E_{\mathrm{swoff}(2)} = \int_{t_1}^{t_2} v_{\mathrm{ce}} i_{\mathrm{ce}} dt = \int_0^{t_{\mathrm{ur}}} \left(\frac{V_{\mathrm{dc}}}{t_{\mathrm{ur}}} t\right)\left(I_o - \frac{2V_{\mathrm{dc}}}{t_{\mathrm{ur}} R_{s1}} t\right) dt = \left(\frac{V_{\mathrm{dc}} I_o}{2} - \frac{2V_{\mathrm{dc}}^2}{3R_{s1}}\right) t_{\mathrm{ur}}. \quad (12)$$

Mode III [t_2, t_3]: At t_2 moment, v_{ce} reaches V_{dc}, and v_{ce2} falls to zero. The diode D_2 is conducting so that i_{ce} can rapidly decline. The i_{ce} fall time t_{if} can be detected from the datasheet of IGBT, and the power loss during mode III $E_{\mathrm{swoff}(3)}$ can be calculated as follows:

$$E_{\mathrm{swoff}(3)} = \int_{t_2}^{t_3} v_{ce} i_{ce} dt = \int_{t_2}^{t_2+t_{\mathrm{if}}} V_{\mathrm{dc}} \left(i_{\mathrm{ce}}(t_2) - \frac{i_{\mathrm{ce}}(t_2)}{t_{\mathrm{if}}} t\right) dt = V_{\mathrm{dc}} t_{\mathrm{if}} \left(\frac{I_o}{2} - \frac{V_{\mathrm{dc}}}{R_{s1}}\right). \quad (13)$$

Mode IV [after t_3]: After t_3 moment, i_{cs} falls to zero and v_{cs} rises to V_{dc} according to the rule of first-order *RC* full response. D_2 keeps I_{o} in a continuous flow. The IGBT is completely turned off.

During the IGBT turn off, if S is kept opening, IGBT will turn off on a weak absorption trajectory. The turn-off loss of the weak absorption trajectory E_{weakoff} can be calculated from (12) and (13) as follows:

$$E_{\mathrm{weakoff}} = E_{\mathrm{swoff}(2)} + E_{\mathrm{swoff}(3)}. \quad (14)$$

Taking the IGBT module 2MBI1000VXB-170EA-50 ($V_{\mathrm{ce}} = 1700$ V, $I_{\mathrm{ce}} = 1000$ A) of Fuji Electric as an example, the relationship between E_{weakoff} and the snubber resistance R_{s} under the rated condition of the IGBT module can be calculated by (14). Then, $E_{\mathrm{weakoff}}(R_s)$ is normalized with the turn-off loss of hard switching E_{hardoff} ($R_{\mathrm{s}} = \infty$), and the result is shown in Fig. 9. It can be seen that the larger the R_s, the closer the E_{weakoff} is to E_{hardoff}.

Generally, the resistance value of the *RCD* snubber has mainly two restrictions. The first limits the discharge current peak of the snubber capacitor, and the second ensures that the energy of the snubber capacitor can be completely released during the minimum conduction time. Mohan *et al.* [16] have derived the resistance range, as shown in (15). The turn-off loss of the IGBT works on a weak absorption trajectory, which will affect the smoothing ability of the TTAC. In order to maximize the smoothing ability of the TTAC, the resistance in the TTAC can take the largest value in (15) according to Fig. 9

$$\frac{V_{\mathrm{dc}}}{0.2I_o} < R_s < \frac{t_{\mathrm{on(min)}}}{2.3C_s}. \quad (15)$$

B. Effect of Capacitance Value on Turn-off Loss

The snubber resistance value determines the maximum turn-off loss of the IGBT with the TTAC according to Section IV-A. The snubber capacitor value determines the minimum turn-off loss of the IGBT. The TTAC dynamic adjusts of the turn-off loss of an IGBT in this range. So the reduced turn-off loss of a snubber capacitor is very important to estimate the adjustment ability of the TTAC. The relationship between capacitance value and turn-off loss in the ideal case is deduced, as shown in Fig. 10 [19], [20].

In practice, however, the reduction turn-off loss by a snubber capacitor is also affected by other factors, the reduction turn off is much less than it is shown in Fig. 10. During the turn-off of the IGBT, S is kept closing. Since di/dt on the capacitor branch is very large, parasitic inductance cannot be ignored, the equivalent circuit is shown in Fig. 11(a). The induced voltage caused by the parasitic inductance will affect the turn-off loss. In addition, if IGBT is parallel to the capacitor between the collector and emitter, the IGBT trailing current will be changed. Considering the influence of parasitic inductance and tail current, the waveforms of voltage and current during the IGBT turn-off are shown in Fig. 11(b). The phenomenon of tail current is explained in [21] and [22], and the turn-off loss of the IGBT with a snubber capacitor is affected by this phenomenon. Petterteig *et al.* [23] tested the turn-off loss of the IGBT with different parallel capacitors, as shown in Fig. 12. The straight dashed line in Fig. 12 is the loss of the snubber capacitor.

In Fig. 12, the capacitance value and turn-off loss are in accordance with an exponential distribution. The larger the snubber capacitor, the lower the turn-off loss. However, the capacitor

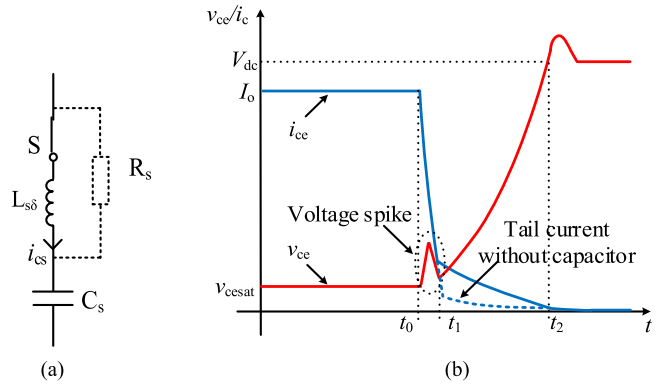

Fig. 11. Turn-off waveform with *RCD* snubber. (a) Equivalent circuit. (b) Waveforms of voltage and current.

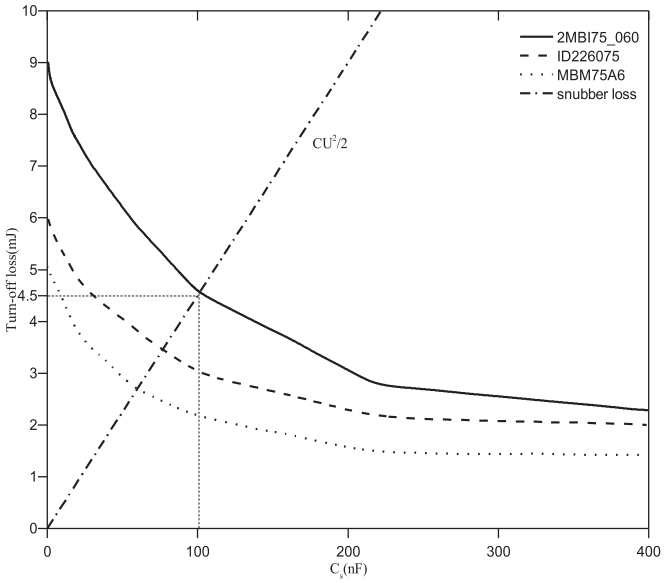

Fig. 12. Turn-off losses as a function of snubber capacitor. $I_{\rm off} = 75$ A, $V_{\rm dc} = 300$ V, and $T_j = 125\,^{\circ}$C.

energy will be consumed in the snubber resistor. With the capacitance value increasing, higher energy is absorbed by the capacitor, and the capacitance value needs to consider the limits of cooling the resistor. The resistor is better mounted on a separate heat sink in order not to affect the temperature of the IGBT. So the selection of the snubber capacitance value needs to have a tradeoff between the snubber circuit loss and smoothing ability of the TTAC.

The turn-off loss of the IGBT with a snubber capacitor that makes the IGBT works on a strong absorption trajectory, $E_{\rm strongoff}$, can be written as follows:

$$E_{\rm strongoff} = kE_{\rm hardoff}\ (k < 1)\,. \tag{16}$$

k is the coefficient that how much the turn-off loss can be reduced by a snubber capacitor, i.e., the snubber capacitor actually reduced the amount of the turn-off loss. Since the reduction turn-off loss by a snubber capacitor is serious affected by many factors, and these factors are all determined by the practical application so that k should not be obtained by the theoretical calculation as shown in Fig. 9 but by calculating the ratio of

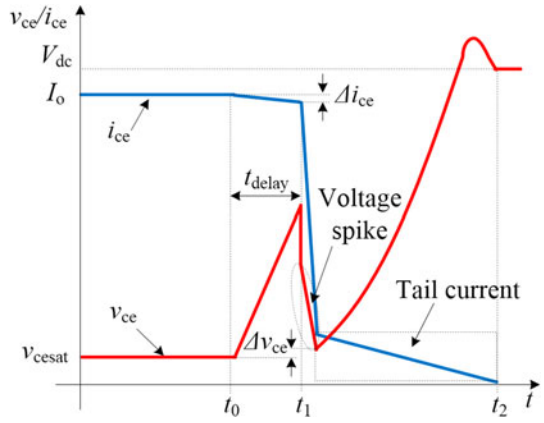

Fig. 13. IGBT turn-off waveform with the parasitic parameter.

$E_{\rm strongoff}$ to $E_{\rm weakoff}$. $E_{\rm strongoff}$ and $E_{\rm weakoff}$ can be obtained by measuring the turn-off waveform of voltage and current with and without the snubber capacitor. k is mainly used to estimate the smoothing ability of the TTAC without the need for extraordinarily precise so that k can be conveniently obtained by actual measurements.

C. Relationship Between $T_{\rm delay}$ and Turn-off Loss

Considering the effect of a snubber capacitor on turn-off loss, the turn-off waveform of the IGBT with the TTAC is shown in Fig. 13. The turn-off loss after adjustment of the IGBT $E_{\rm adjust}(t_{\rm delay})$ is composed of the turn-off loss $E_{\rm weakoff}(t_{\rm delay})$ in the $t_0 - t_1$ stage, in which the IGBT works on a weak absorption trajectory, and the turn-off loss $E_{\rm strongoff}$ in the $t_1 - t_2$ stage, in which the IGBT works on a strong absorption trajectory. Such as the analysis of Section IV-A, if the snubber resistor is large enough, $i_{\rm ce}$ will shunt slightly to the *RC* branch so that $i_{\rm ce}$ and $v_{\rm ce}$ will have a little change as shown in the Fig. 13, there is a little change in $E_{\rm strongoff}$ as well. Therefore, the influence of $t_{\rm delay}$ on $E_{\rm strongoff}$ is ignored in order to simplify the calculation. From (12) and (16), the relationship between $t_{\rm delay}$ and $E_{\rm adjust}(t_{\rm delay})$ can be calculated as follows. The relationship between $t_{\rm delay}$ and turn-off loss can be used for the decision-making algorithm of the TTAC control

$$E_{\rm adjust}(t_{\rm delay}) = E_{\rm weak}(t_{\rm delay}) + E_{\rm strongoff} = \left(\frac{V_{\rm dc}I_o}{2t_{\rm ur}}t_{\rm delay}^2 - \frac{2V_{\rm dc}^2}{3t_{\rm ur}^2R_s}t_{\rm delay}^3\right) + kE_{\rm hardoff},\ (t_{\rm delay} < t_{\rm ur}, k < 1)\,. \tag{17}$$

V. Smoothing Ability Estimation Method of the TTAC

The smoothing ability of the TTAC means the maximum proportion of the load fluctuation accounts for the rated load and that the internal loss of the IGBT can be kept stable by the TTAC. In this section, the estimation method for the smoothing ability of the TTAC is deduced. This method enables estimating the smoothing ability of the TTAC under different operating conditions by the IGBT datasheet.

TABLE I
PARAMETERS OF 1.2-MW WIND CONVERSION SYSTEM

Parameters	Value
Rated power (MW)	1.2
DC bus (V)	1100
Grid voltage (V)	690
Rated frequency of grid side converter (Hz)	50
Switching frequency (kHz)	5
Modulation	SPWM

First, the switching energy loss $E_{\mathrm{hardon}}(V_{\mathrm{dc}}, i_{\mathrm{ce}}, T_j, f_s)$, $E_{\mathrm{hardoff}}(V_{\mathrm{dc}}, i_{\mathrm{ce}}, T_j, f_s)$, in which the IGBT works on hard switching, and the conduction energy loss $E_{\mathrm{con}}(V_{\mathrm{dc}}, i_{\mathrm{ce}}, T_{\mathrm{j}})$ are estimated by the datasheet of the IGBT. Second, the average power loss $P_{\mathrm{hardon}}(V_{\mathrm{dc}}, i_{\mathrm{ce}}, T_j, f_s)$, $P_{\mathrm{hardoff}}(V_{\mathrm{dc}}, i_{\mathrm{ce}}, T_j, f_s)$, and $P_{\mathrm{con}}(V_{\mathrm{dc}}, i_{\mathrm{ce}}, T_{\mathrm{j}})$ of the IGBT in a fundamental cycle is estimated according to the energy loss and the modulation of the converter. At last, the smoothing ability of the TTAC can be estimated by the average power loss with strong and weak absorption trajectories. Taking the IGBT module used in a 1.2-MW direct-drive wind power converter as an example, the converter parameters are shown in Table I. The selected IGBT module is 2MBI1000VXB-170EA-50 ($V_{\mathrm{ce}} = 1700$ V, $I_{\mathrm{ce}} = 1000$ A) manufactured by Fuji Electric.

The i_{ce}–v_{cesat} curve and the switching loss curve in the datasheet can be fitted by a polynomial, and the fitting results are shown in Fig. 14. The relationship between i_{ce} and v_{cesat} can be written as follows:

$$v_{\mathrm{cesat}} = R_{\mathrm{ce}} i_{\mathrm{ce}} + V_{\mathrm{ce0}}. \tag{18}$$

Here, $R_{\mathrm{ce}} = \Delta v_{\mathrm{cesat}}/\Delta i_{\mathrm{ce}}$ is the on resistance, and v_{ce0} is v_{cesat} when $i_{\mathrm{ce}} = 0$.

We assume that R_{ce}, V_{ce0}, and junction temperature T_{j} satisfy a linear relationship. According to the $i_{\mathrm{ce}} - v_{\mathrm{cesat}}$ curves of 25 and 150 °C which are given by the datasheet, the relationship among R_{ce}, V_{ce0}, and T_{j} can be acquired by the interpolation method

$$V_{\mathrm{ce0}}(T_j) = \frac{V_{\mathrm{ce0(150\,^\circ C)}} - V_{\mathrm{ce0(25\,^\circ C)}}}{100}(T_j - 25) + V_{\mathrm{ce0(25\,^\circ C)}} \tag{19}$$

$$R_{\mathrm{ce}}(T_j) = \frac{R_{\mathrm{ce(150\,^\circ C)}} - R_{\mathrm{ce(25\,^\circ C)}}}{100}(T_j - 25) + R_{\mathrm{ce(25\,^\circ C)}}. \tag{20}$$

The relationship among V_{dc}, i_{ce} and E_{hardon}, E_{hardoff} can be written as follows:

$$E_{\mathrm{hardon}}(V_{\mathrm{dc}}, i_{\mathrm{ce}}) = ({p_1}^* i_{\mathrm{ce}}^2 + {p_2}^* i_{\mathrm{ce}} + p_3) V_{\mathrm{dc}}/V_{\mathrm{dc}N} \tag{21}$$

$$E_{\mathrm{hardoff}}(V_{\mathrm{dc}}, i_{\mathrm{ce}}) = ({p_4}^* i_{\mathrm{ce}}^2 + {p_5}^* i_{\mathrm{ce}} + p_6) V_{\mathrm{dc}}/V_{\mathrm{dc}N}. \tag{22}$$

Here, p_1–p_6 are the fitting coefficients, and $V_{\mathrm{dc}N}$ is the dc-bus voltage in Fig. 14 (b).

We assume that the switching loss and T_{j} also satisfy a linear relationship. According to the switching loss curves of 25 and 150 °C, the relationship between E_{hardoff}, E_{hardon}, and T_j can also be acquired by the interpolation method

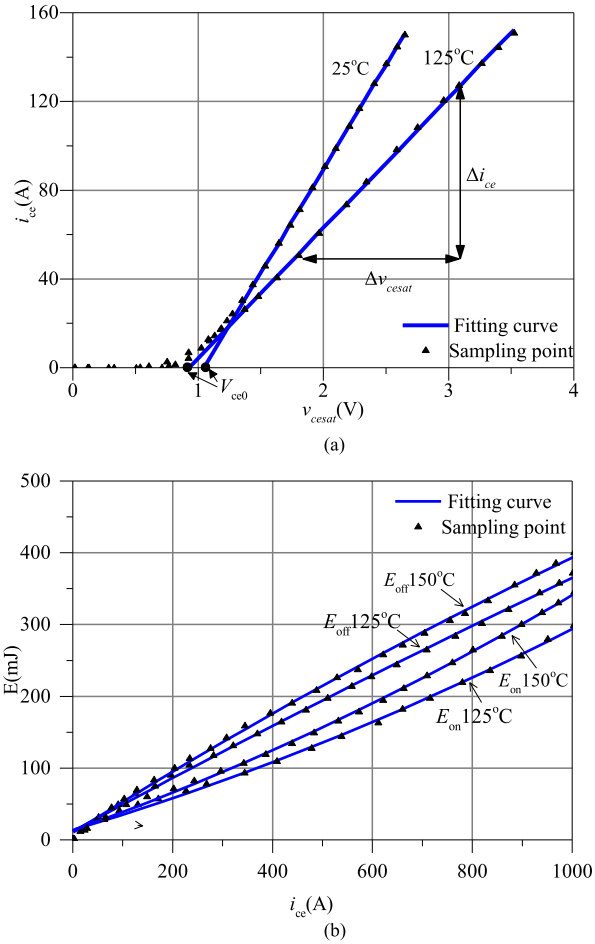

Fig. 14. Result of data fitting. (a) Output characteristic. (b) Switching losses (the dc-bus voltage $V_{\mathrm{dc}N}$ is 600 V).

$$E_{\mathrm{hardoff}}(V_{\mathrm{dc}}, i_{\mathrm{ce}}, T_j) = \frac{E_{\mathrm{hardoff(150^\circ)}} - E_{\mathrm{hardoff(125^\circ)}}}{25}$$
$$(T_j - 125) + E_{\mathrm{hardoff(125^\circ)}} = ({\mu_1}^* i_{\mathrm{ce}}^2 + {\mu_2}^* i_{\mathrm{ce}} + \mu_3) V_{\mathrm{dc}}/V_{\mathrm{dc}N} \tag{23}$$

$$E_{\mathrm{hardon}}(V_{\mathrm{dc}}, i_{\mathrm{ce}}, T_j) = \frac{E_{\mathrm{hardon(150^\circ)}} - E_{\mathrm{hardon(125^\circ)}}}{25}$$
$$(T_j - 125) + E_{\mathrm{hardon(125^\circ)}} = ({\mu_4}^* i_{\mathrm{ce}}^2 + {\mu_5}^* i_{\mathrm{ce}} + \mu_6) V_{\mathrm{dc}}/V_{\mathrm{dc}N}. \tag{24}$$

Here, μ_1–μ_6 are the simplified coefficients.

P_{hardon}, P_{hardoff}, and P_{con} of IGBT when the converter works on SPWM modulation are deduced [24]. From (19), (20), the relationship among I_{load}, T_j, and P_{con} can be written as follows:

$$P_{\mathrm{con}}(I_{\mathrm{load}}, T_j) = \frac{1}{2}\left(V_{\mathrm{ce0}}\frac{I_{l\max}}{\pi} + R_{\mathrm{ce}}\frac{I_{l\max}^2}{4}\right) - m \cdot \cos\varphi \cdot \left(V_{\mathrm{ce0}}\frac{I_{l\max}}{8} + R_{\mathrm{ce}}\frac{I_{l\max}^2}{3\pi}\right). \tag{25}$$

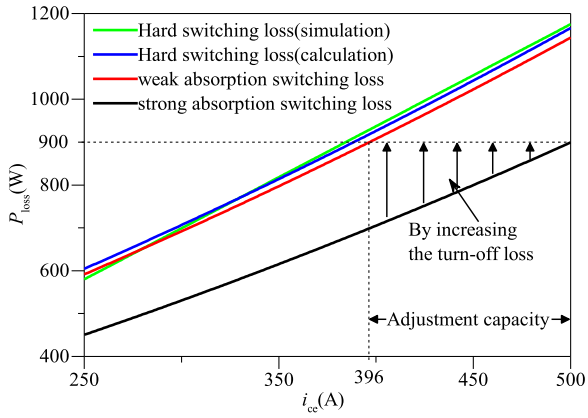

Fig. 15. Smoothing ability of the TTAC.

Here, $I_{lmx} = \sqrt{2}I_{load}$ is the peak value of the load current, and φ is the power factor.

According to the result from (23), (24), $P_{hardon}(V_{dc}, i_{ce}, T_j, f_s)$, $P_{hardoff}(V_{dc}, i_{ce}, T_j, f_s)$ can be written as follows:

$$P_{hardon}(V_{dc}, I_{load}, T_j, f_s) = f_s\left(\frac{\mu_1 I_{lmx}^2}{4} + \frac{\mu_2 I_{lmx}}{\pi} + \frac{\mu_3}{2}\right) V_{dc}/V_{dcN} \quad (26)$$

$$P_{hardoff}(V_{dc}, I_{load}, T_j, f_s) = f_s\left(\frac{\mu_4 I_{lmx}^2}{4} + \frac{\mu_5 I_{lmx}}{\pi} + \frac{\mu_6}{2}\right) V_{dc}/V_{dcN}. \quad (27)$$

As shown by the blue line in Fig. 15, the relationship between I_{load} and the power loss of hard switching P_{hard} is acquired by substituting (25)–(27) into (1). The green line in Fig. 15 gives the simulation results from Fuji Electronic loss simulation software [17]. It can be seen that the calculation results by (1) are in good agreement with the simulation results, i.e., the result of (1) is trustworthy. The resistor of the TTAC is set to 75 Ω, and the turn-off power loss of the weak absorption trajectory $P_{weakoff}$ is 95.8% of $P_{hardoff}$ from (14). The total power loss of the weak absorption trajectory P_{weak} can be written as (28). The total power loss of the strong absorption trajectory P_{strong} can be written as (29) from (16)

$$P_{weak}(V_{dc}, I_{load}, T_j, f_s) = P_{con}(I_{load}, T_j) + P_{hardon} \times (V_{dc}, I_{load}, T_j, f_s) + 0.958P_{hardoff}(V_{dc}, I_{load}, T_j, f_s) \quad (28)$$

$$P_{strong}(V_{dc}, I_{load}, T_j, f_s) = P_{con}(I_{load}, T_j) + P_{hardon} \times (V_{dc}, I_{load}, T_j, f_s) + kP_{hardoff}(V_{dc}, I_{load}, T_j, f_s). \quad (29)$$

According to (28), (29), the relationship between the power losses (P_{weak}, P_{strong}) and I_{load} are shown by the red line and black line in Fig. 15 (assuming $k = 0.5$), i.e., the power loss of the IGBT can be adjusted between the red line and the black line under the same load current by the TTAC. It can be seen that the power loss is 900 W when the IGBT works on a strong absorption trajectory with a 500-A load current. Moreover, the power loss can be maintained at 900 W by the TTAC when the load current fluctuates between 396 and 500 A. This means that the internal loss of the IGBT can be kept constant, and the junction temperature can be smoothed by the TTAC when the fluctuation of the load is within 20.8% of the rated power (396–500 A).

TABLE II
ADJUSTMENT ABILITY OF DIFFERENT k

Parameters	Value				
k	0.5	0.4	0.3	0.2	0.1
Adjustment ability	19%	25.6%	30.4%	35.4%	40.2%

If the TTAC can be fitted with a larger snubber capacitor, the adjustment ability of the TTAC will be extended. The adjustment ability of TTAC with different k (in (16)) is given by Table II. The TTAC can smooth the junction temperature fluctuation caused by a 40.2% rated load fluctuation when k is 0.1.

VI. EXPERIMENTAL VERIFICATION

At present, online junction temperature measurement is still a difficult problem, so the existing active junction temperature control has widely used the look-up table according to the load current, and to verify the effectiveness of active junction temperature control, the junction temperature usually be measured using an infrared radiation camera (IR) on the open IGBT module. This paper adopts the same method to the experimental verification.

A high-power IGBT that requires more active junction temperature control is typically used in bridge topologies. The experimental validation is done on a single-phase two-level inverter in H-bridge topology with a TTAC, as shown in Fig. 16(a) (the shadow box represents the other TTACs). The components model in Fig. 16(a) is shown in Table III. To enable direct temperature measurement by IR, an opened IGBT module is used without filling gel. This module is provided by the manufacturer Fuji Electric. The insulation voltage of the opened IGBT module is significantly reduced because no gel is filled, so the experimental bus voltage is set to 200 V. The major parameters of the inverter are shown in Table IV. The control of the inverter and the TTAC is implemented on a DSP development board. The setup of the experiment platform and the TTAC is shown in Fig. 16(b) and (c).

A. Validation of Switch Trajectory

In Fig. 16(a), the turn-on signal of the auxiliary switch S delays the turn-off signal of the main switch T_1 for 397 ns (i.e., $t_{dealy} = 397$ ns). The T_1 experimental waveforms of voltage and current measured by a differential voltage probe and Rogowski coil are shown in Fig. 17(a). At t_0 moment, S is kept opening, and T_1 works on a weak absorption trajectory. At t_1 moment, S is closed, v_{ce} suddenly drops to the capacitor voltage, and i_{ce} begins to rapidly decline. T_1 works on a weak absorption trajectory. In the $t_0 - t_1$ stage, i_{ce} has fallen 4.4 A from

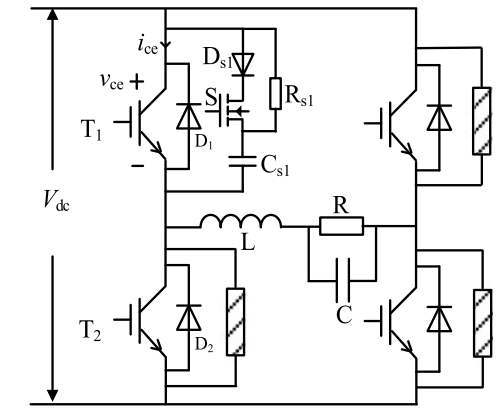

(a)

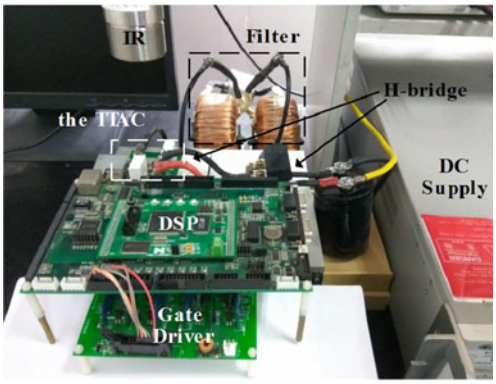

(b)

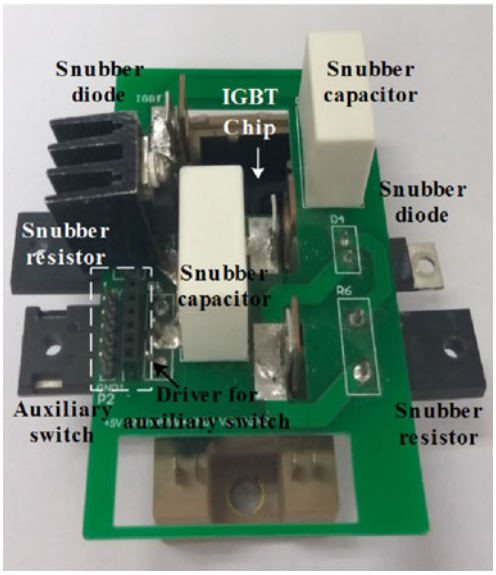

(c)

Fig. 16. Experiment platform for thermal management. (a) Principle diagram of the experiment system. (b) Experiment platform. (c) TTAC.

I_o. According to (3), the change of v_{ce} should be 165 V, which conforms to the experimental measurements.

The T_1 experimental waveforms of voltage and current with different t_{delay} are shown in Fig. 17(b) and (c). It can be seen that T_1 starts to work on a weak absorption trajectory. After S is closed, v_{ce} suddenly drops to the capacitor voltage, i_{ce} begins to rapidly decline, and T_1 works on a weak absorption trajectory.

TABLE III
COMPONENTS MODEL

Components	Manufacturer	Model
IGBT module	FUJI ELECTRIC	2MBI75VA120 (1200 V/75 A)
D_{s1}	Infineon	IDH10G120C5 (1200 V/10 A)
R_{s1}	Ohmite	AP101 75R (75 Ω/100 W)
C_{s1}	EACO	STC-1200-0.1 (0.1 μF/1200 V)
S (MOSFET)	Infineon	IPW65R310CFD (700 V/11.4 A)
C (filter capacitor)	EACO	SHA-700-35 (35 μF/700 V)
L (filter inductor)	Customize	2 mH

TABLE IV
MAIN CIRCUIT PARAMETERS OF INVERTER

Parameters	Value
Input voltage	200 V
Output voltage	110 V
Rated current	33 A
Output line frequency	50 Hz
Switching frequency	20 kHz

The principle analysis of the TTAC in Section III is verified by the experimental results.

The principle of the TTAC shows that the auxiliary switch only works for charging the snubber capacitor, and it is opened after the charging accomplished, so it turns off at zero current switching. As a result, the auxiliary switch produces loss only during the process of capacitor charging and no the turn-off losses. Due to the snubber capacitor is very small, the auxiliary switch only needs to conduct very short time, so the auxiliary switch can be determined by the repetitive pulse current of a power switch. Taking Semikron's IGBT4 as an example, the repetitive pulse current I_{CRM} of an IGBT4 can be set to three times of rated current I_{Cnom}, i.e., $I_{CRM} = 3^* I_{Cnom}$ [25]. So that as the setup of Table I, the current rating of the auxiliary switch will be set to 1000/3 ≈ 400 A, e.g., the IGBT module SKM400GB17E4 ($V_{ce} = 1700$ V, $I_{ce} = 400$ A) manufactured by Semikron. Its repetitive pulse current is 1200 A and can sustain 10 μs according to the datasheet. As the experiment setup, the MOSFET IPX65R310CFD ($V_{ce} = 650$ V, $I_{ce} = 11.4$ A) manufactured by Infineon has been selected. Its repetitive pulse current is 34 A and can sustain for 1 ms according to its datasheet.

The experimental waveforms with the auxiliary switch for two switching cycles (switching frequency is 20 k) are shown in Fig. 18, the t_{dealy} is also set to 397 ns. It can be seen that the auxiliary switch produces once loss in each switch cycle and the duration is very short. The enlarged waveforms of the dashed box show the loss of the auxiliary switch only includes turn-on loss and conduction loss. Compared with the main switch, the conduction loss of the auxiliary switch can be ignored, the turn-on loss is less due to the auxiliary switch will be closed before v_{ce} arrives at V_{dc} and there is no turn-off loss in the auxiliary switch so that the loss of the auxiliary switch is much less than the loss of the main switch. In addition, the life consumption of the junction temperature fluctuations at the switching frequency for

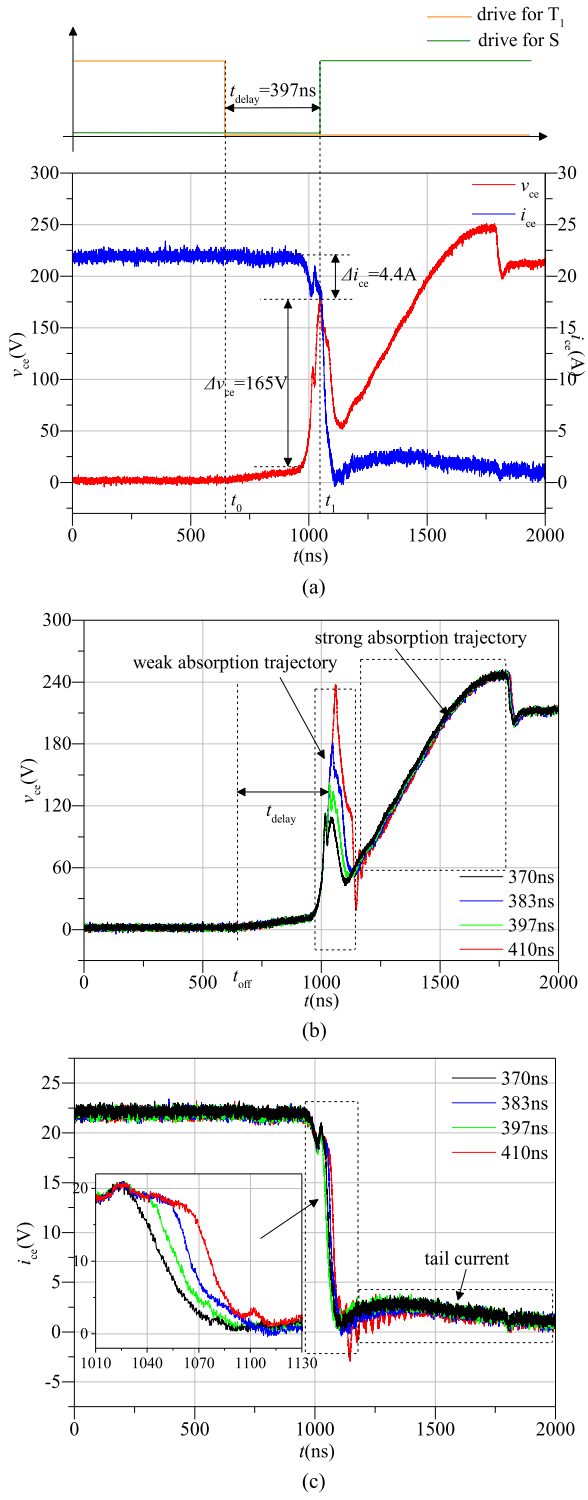

Fig. 17. Experimental waveforms of the TTAC. (a) t_{delay} is 397 ns. (b) v_{ce} waveforms with different t_{delay}. (c) i_{ce} waveforms with different t_{delay}.

a semiconductor can be ignored [7], and the average loss power of the auxiliary switch is much lower than the main switch. So that the thermal stress of the auxiliary switch is much lower than the main switch, and the life expectancy of the auxiliary switch is much higher than the main switch. What's more, if the auxiliary switch is short, then the TTAC is a *RCD* snubber; if the auxiliary

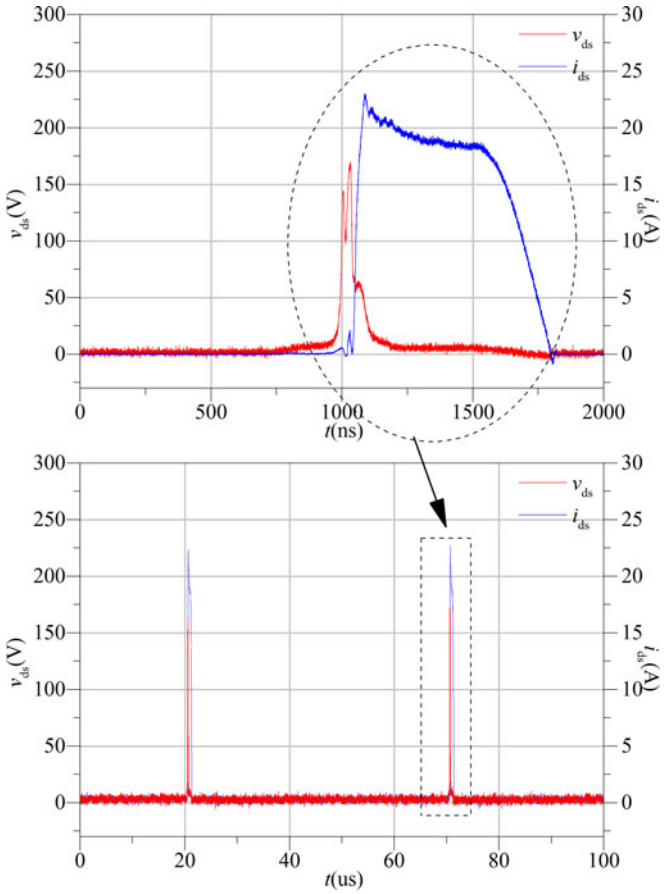

Fig. 18. Experimental waveforms of the auxiliary switch.

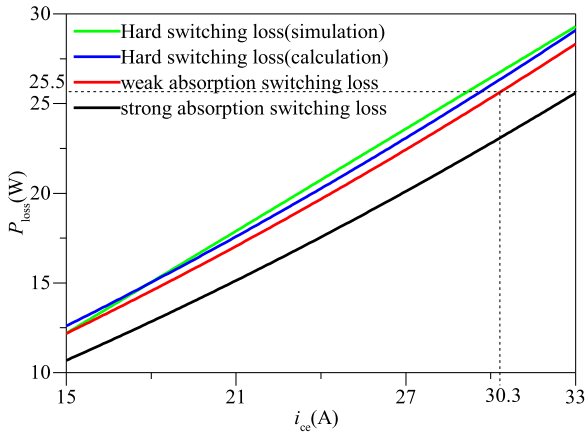

Fig. 19. TTAC smoothing ability of 2MBI75VA120.

switch is broken, then the TTAC is a *RC* snubber, as shown in Fig. 18, neither of them will affect the normal operation of the main circuit. So it does not introduce a new security risk.

B. Smoothing Ability of the TTAC

The snubber capacitor is set to 100 nF in this experiment, and it can reduce 46% the turn-off loss of hard switching, i.e., k is 0.54 in (29). According to the estimation method in Section V, the smoothing ability of the TTAC is shown in Fig. 19. The

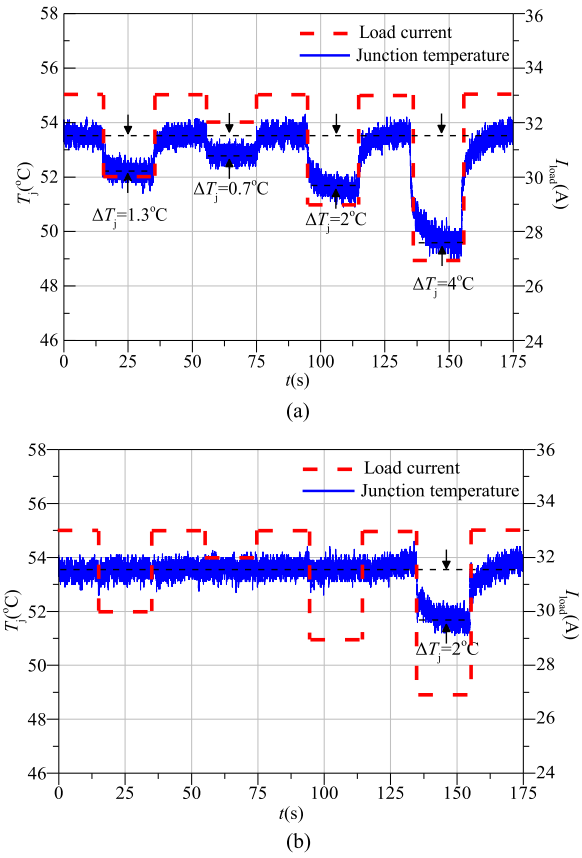

Fig. 20. Junction temperature profile with and without the TTAC: (a) Without the TTAC. (b) With the TTAC.

power loss can be maintained at 25.5 W by the TTAC when the load current fluctuates between 30.3 and 33 A. This means that the junction temperature can be smoothed by the TTAC when the load fluctuation is within 8.2% of the rated power (30.3–33 A).

In the junction temperature smoothing experiment, the load current is set to a square wave to represent random fluctuation, as shown in Fig. 20(a). The load current fluctuates in the form of 33-30-33-32-33-29-33-27 A, with a 20-s interval, and the junction temperature will follow the load fluctuation without the active junction temperature control.

The $t_{\mathrm{delay}}s$ are calculated by (17) according to the load current, which are placed in a look-up table for the TTAC control. The profile of the junction temperature with the TTAC is shown in Fig. 20(b). The TTAC can completely smooth the temperature fluctuations when the load fluctuations are 12% (29 A) or less of the rated load (33 A); and the TTAC can reduce the temperature fluctuations when the load fluctuations are more than 12% (27 A). ΔT_j is decreased from 4 to 2 °C. The experimental smoothing ability of the TTAC (12%) is larger than the theoretical value (8.2%) in Fig. 19. This is because the theoretical value does not consider the impact of parasitic inductance on the turn-on loss. The experimental turn-on loss is smaller than the theoretical value, and, in fact, the turn-off loss accounts for a larger proportion of the total loss.

VII. Conclusion

In this paper, an active junction temperature control method is proposed by adjusting the turn-off loss. The turn-off loss is adjusted by the IGBT turn-off trajectory that is shifted by the TTAC. The effects of the snubber resistor and the snubber capacitor on the turn-off loss were investigated. The method of estimating the TTAC smoothing ability under different operating conditions was deduced. Using an IGBT applied in a 1.2-MW wind power converter as an example, the junction temperature fluctuation caused by 40% of the rated load fluctuation can be smoothed by the TTAC, as shown by the estimation result.

A low-power experiment was implemented. The experimental results showed that the turn-off trajectory of the IGBT with the TTAC was consistent with the principle analysis in Section III, and the turn-off trajectory can be shifted from weak absorption to strong absorption by controlling the auxiliary switch. Experimental comparisons of temperature profiles with and without the TTAC showed that the junction temperature fluctuation can be smoothed or reduced by the TTAC. The method of estimating the smoothing ability in Section V was also validated. The actual smoothing ability of the TTAC conformed to the theoretical value, and the actual smoothing ability may be greater than the theoretical value due to the parasitic inductance reducing the turn-on loss.

Compared to existing active junction temperature control methods, such as switching frequency and gate control, the TTAC can individually adjust the loss of each IGBT in the bridge topology and does not introduce a new security risk. The costs of this method are to increase the volume and expense, and the adjustment range is limited by the dc-bus voltage due to the turn-off loss is affected by the dc-bus voltage, but these costs are relatively low according to the previous analysis. The method will significantly improve the junction temperature stabilization of an IGBT, if those costs can be accepted.

References

[1] F. Spinato *et al.*, "Reliability of wind turbine subassemblies," *IET Renew. Power Gener.*, vol. 3, no. 4, pp. 387–401, 2009.
[2] J. Ribrant and L. M. Bertling, "Survey of failures in wind power systems with focus on Swedish wind power plants during 1997–2005," *IEEE Trans. Energy Convers.*, vol. 22, no. 1, pp. 167–173, Mar. 2007.
[3] M. Boettcher and F W. Fuchs, "Power electronic converters in wind energy systems—Considerations of reliability and strategies for increasing availability," in *Proc. 2011 14th Eur. Conf. Power Electron. Appl.*, 2011, pp. 1–10.
[4] J. Lutz, "IGBT-modules: Design for reliability," in *Proc. IEEE 13th Eur. Conf. Power Electron. Appl.*, Barcelona, Spain, 2009, pp. 1–3.
[5] M. Ciappa, "Selected failure mechanisms of modern power modules," *Microelectron. Rel.*, vol. 42, nos. 4/5, pp. 653–667, 2002.
[6] R. Bayerer *et al.*, "Model for power cycling lifetime of IGBT modules—Various factors influencing lifetime," in *Proc. 5th Int. Conf. Integr. Power Electron. Syst.*, 2008, pp. 1–6.
[7] Z. Zhou *et al.*, "High-speed electro-thermal simulation model of inverter power modules for hybrid vehicles," *IET Electr. Power Appl.*, vol. 5, no. 8, pp. 636–643, 2011.
[8] X. Du *et al.*, "Multi-time scale lifetime evaluation of IGBT modules in the wind power converter," *Proc. CSEE*, vol. 35, no. 23, pp. 6152–6161, 2015.
[9] J. Wu *et al.*, "Smooth control of insulated gate bipolar transistors junction temperature in a small-scale wind power converter," *IET Power Electron.*, vol. 9, no. 3, pp. 393–400, 2016.

[10] J. Falck, M. Andresen, and M. Liserre, "Active thermal control of IGBT power electronic converters," in *Proc. 2015 41st Annu. Conf. IEEE Ind. Electron. Soc.*, 2015, pp. 000001–000006.
[11] P. K. Prasobhu, G. Buticchi, S. Brueske, and M. Liserre, "Gate driver for the active thermal control of a dc/dc GAN-based converter," in *Proc. 2016 IEEE Energy Convers. Congr. Expo.*, 2016, pp. 1–8.
[12] K. Ma, M. Liserre, and F. Blaabjerg, "Reactive power influence on the thermal cycling of multi-MW wind power inverter," *IEEE Trans. Ind. Appl.*, vol. 49, no. 2, pp. 922–930, Mar./Apr. 2013.
[13] K. Ma and F. Blaabjerg, "Modulation methods for neutral-point-clamped wind power converter achieving loss and thermal redistribution under low-voltage ride-through," *IEEE Trans. Ind. Electron.*, vol. 61, no. 2, pp. 835–845, Feb. 2014.
[14] M. Andresen, G. Buticchi, and M. Liserre, "Thermal stress analysis and MPPT optimization of photovoltaic systems," *IEEE Trans. Ind. Electron.*, vol. 63, no. 8, pp. 4889–4898, Aug. 2016.
[15] X. Wang, A. Castellazzi, and P. Zanchetta, "Regulated cooling for reduced thermal cycling of power devices," in *Proc. 2012 7th Int. Power Electron. Motion Contr. Conf.*, Jun. 2012, vol. 1, pp. 238–244.
[16] N. Mohan, T. M. Undeland, and W. P. Robbins, *Power Electronics: Converters, Applications, and Design*, 3rd ed. New York, NY, USA: Wiley, 2003.
[17] *Fuji IGBT Simulator (Ver. 6.0.5) [EB/OL]*. [Online]. Available: http://www.fujielectric.com/products/semicon-ductor/model/igbt/simulation/index.html
[18] M. Trivedi and K. Shenai, "Modeling the turn-off of IGBT's in hard- and soft-switching applications," *IEEE Trans. Electron Devices*, vol. 44, no. 5, pp. 887–893, May 1997.
[19] E. T. Calkin and H. Hamilton, "Circuit techniques for improving the switching loci of transistor switches in switching regulators," *IEEE Trans. Ind. Appl.*, vol. IA-12, no. 4, pp. 364–369, Jul./Aug. 1976.
[20] W. McMurray, "Selection of snubbers and clamps to optimize the design of transistor switching converters," *IEEE Trans. on Ind. Appl.*, vol. IA-16, no. 4, pp. 513–523, Jul./Aug. 1980.
[21] M. Trivedi, S. Pendharkar, and K. Shenai, "Switching characteristics of MCT's and IGBT's in power converters," *IEEE Trans. Electron Devices*, vol. 43, no. 11, pp. 1994–2003, Nov. 1996.
[22] I. Widjaja *et al.*, "Switching dynamics of IGBTs in soft-switching converters," *IEEE Trans. Electron Devices*,, vol. 42, no. 3, pp. 445–454, Mar. 1995.
[23] A. Petterteig, J. Lode, and T. M. Undeland, "IGBT turn-off losses for hard switching and with capacitive snubbers," in *Proc. Conf. Rec. 1991 IEEE Ind. Appl. Soc. Annu. Meet.*, 1991, pp. 1501–1507.
[24] W. Pan *et al.*, "Dissipation analysis of VSC-HVDC converter," *Proc. CSEE*, vol. 28, no. 21, pp. 7–14, 2008.
[25] A. Wintrich, U. Nicolai, W. Tursky, and T. Reimann, *Semikron, Application Manual Power Semiconductors*, ISLE GmbH, Ilmenau, Germany, 2011.

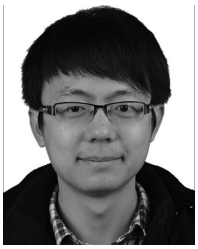

Bo Wang received the B.E. degree in automation from Beijing University of Technology, Beijing, China, in 2010, and the M.S. degree in measurement technology and instruments from Chongqing University of Technology, Chongqing, China, in 2013, where he is currently working toward the Ph.D. degree in electrical engineering.

His research interests include reliability and junction temperature management of IGBT.

Luowei Zhou (M'04–SM'04) received the B.S., M.S., and Ph.D. degrees in electrical engineering from Chongqing University, Chongqing, China, in 1982, 1988, and 2000, respectively.

Between September 1998 and August 1999, he was a Visiting Professor with the University of California, Irvine, USA. Since 1982, he has been with the College of Electrical Engineering, Chongqing University, where he is currently a Full Professor. He has published more than 70 papers, is the holder of one U.S. patent and four China patents, and has three patents pending. His major research interests include analysis and control of power electronics circuits, realization of active power filters, power-factor-correction techniques, and high-frequency power conversion.

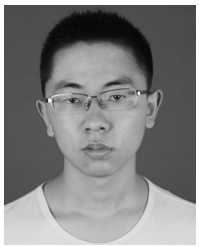

Yi Zhang received the B.S. degree in electrical engineering from Chongqing University, Chongqing, China, in 2015, where he is currently working toward the M.S. degree in electrical engineering.

His research interests include reliability and junction temperature management of IGBT.

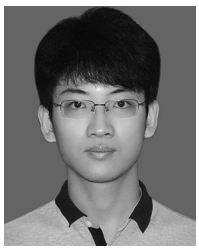

Kaihong Wang received the B.E. and M.S degrees in electrical engineering from Anhui University of Technology, Ma'anshan, China, in 2013 and 2015, respectively. He is currently working toward the Ph.D. degree in electrical engineering at Chongqing University, Chongqing, China.

His research interest focuses on reliability of power electronic module.

Xiong Du (M'13) received the B.S., M.S., and Ph.D. degrees in electrical engineering from Chongqing University, Chongqing, China, in 2000, 2002, and 2005, respectively.

From July 2007 to July 2008, he was a Visiting Scholar with Rensselaer Polytechnic Institute. Since 2002, he has been with Chongqing University, where he is currently a Full Professor with the College of Electrical Engineering. His research interests include switching power converters, power quality control, and renewable energy power conversion.

Dr. Du received the National Excellent Doctoral Dissertation of China in 2008.

Pengju Sun (M'13) received the B.S. and Ph.D. degrees in electrical engineering from Chongqing University, Chongqing, China, in 2005 and 2011, respectively.

Between September 2009 and August 2010, she was a visiting student with the University of California, Irvine, USA. Since 2011, she has been with the College of Electrical Engineering, Chongqing University, where she is currently an Associate Professor. Her research interests include switching power converters, power quality control, and reliability of power converter.